Narrow-band acceleration of gold ions from ultra-thin foils

Contact: p.martin@qub.ac.uk

P. Martin, F. Hanton, D. Gwynne, M. Borghesi, S. Kar
Centre for Plasma Physics, School of Mathematics and Physics, Queen's University Belfast, BT7 1NN, UK

H. Ahmed, J. S. Green
Central Laser Facility, Rutherford Appleton Laboratory, Didcot, Oxfordshire, OX11 0QX, UK

D. Doria
Extreme Light Infrastructure (ELI-NP), and Horia Hulubei National Institute for R&D in Physics and Nuclear Engineering (IFIN-HH), Str. Reatorului No. 30, 077125 Bucharest-Magurele, Romania

D. Maclellan, P. McKenna
Department of Physics, SUPA, University of Strathclyde, Glasgow G4 0NG

M. Cerchez, M. Swantusch, O. Willi
Institut für Laser-und Plasmaphysik, Heinrich-Heine-Universität, Düsseldorf, Germany

A. Alejo
IGFAE, Universidade de Santiago de Compostela, Santiago de Compostela, Spain

J. Fernández-Tobías, J. A. Ruiz
Instituto de Fusion Nuclear, Universidad Politécnica de Madrid, Madrid, Spain

A. Macchi
Istituto Nazionale di Ottica, Consiglio Nazionale delle Ricerche (CNR/INO), Laboratorio Adriano Gozzini, Pisa, Italy

S. Zhai
Department of Mathematics and Physics, Shanghai Normal University, Shanghai 200234, China

Abstract

Interaction of intense lasers with nm thick targets provides an attractive regime for the acceleration of ions of all types. Acceleration of heavy ions however is undermined in the presence of low-Z contaminant species due to their higher charge-to-mass ratio. Here we show a narrow-band acceleration of super-heavy Au ions from ∼15 nm Au foils driven by a sub-Petawatt laser, with spectral peaks of 1.5 ± 0.5 GeV at fluxes on the order of 10^{12} particles per steradian. 2D particle-in-cell simulations show a complex interplay between different acceleration mechanisms at different stages of interaction, suggesting the Au bunches stem from strong radiation pressure acceleration on a heavy-ion dominant plasma in the moments just before transparency, followed by an efficient acceleration due to transparency-enhanced mechanisms.

1 Introduction

Laser-driven ion acceleration has gained substantial interest in recent years [1, 2] due to its potential diverse applications in fields such as radiotherapy [3], high energy density physics [4], and nuclear physics [5]. In particular, the acceleration of extremely heavy ions, e.g. Au, to GeV energies and in high particle numbers has caught attention for nuclear physics research, in the context of, for example, the fission-fusion reaction mechanism to study the astrophysical r-process [6], which demands kinetic energies of several MeV/nucleon [6] and at very high fluxes to be efficient. While laser-driven sources offer the only possible route to deliver these ultra-short bunches of ions, significant progress has been made with high power lasers accelerating heavy ions to multi-MeV/nucleon, albeit, so far, with a broadband, thermal spectrum (attributed to a sheath acceleration dominated interaction) that limits the number of particles at the high energy end of the spectrum [7–15].

In this article, we show results obtained employing ultra-thin Au foils, where very significant acceleration of the heavy bulk species is observed, in spectral peaks of narrow bandwidth. Gold ions were accelerated to energies up to 2 GeV, with pronounced spectral peaks spanning the 1–2 GeV (5–10 MeV/n) range — to our knowledge this is the first instance of bunched acceleration of extremely heavy ions, with a peak particle flux at high energy that is several orders of magnitude greater than what has previously been reported [8, 11, 15]. Particle-in-cell simulations indicate that a multi-mechanism, hybrid acceleration process [17] takes place in stages, where radiation pressure acceleration (RPA) leads to the bunching of Au ions only in the moments close to the onset of transparency, acting

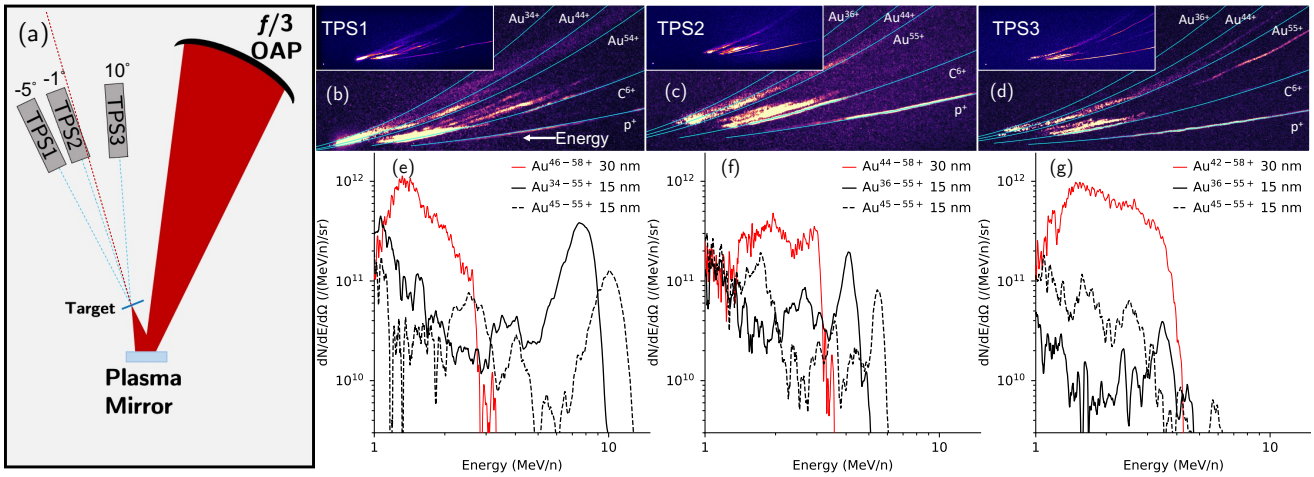

Figure 1: **(a)** Schematic of the experimental setup, TPS1–3 represents the three high resolution Thomson parabola spectrometers (TPS) deployed at different angles (as labelled) with respect to target normal (red dashed line). **(b, c, d)** Raw image plate data from each TPS on 15 nm gold foil, with example ion traces indicated in cyan, where ion energies increase going from right to left on each image. Au ion traces (as labelled) represent the bounds of the charge ranges over which spectra were integrated. The insets show the full IP image. **(e, f, g)** Au ion spectra, in order from TPS1 to TPS3, for 15 nm (black) and 30 nm (red) targets. For both thicknesses, spectra are shown representing signal integration over the entirety of the charge states observed (solid lines, charge ranges are as labelled in the legend), and energies calculated assuming a central charge of 44+ and 51+ for the 15 and 30 nm targets, respectively. Additionally, for the 15 nm target, a second spectrum was generated integrating signal only for charges above 45+ (dashed lines), representing most of the ion signal, at a central charge of 51+. The difference in ion energy at the spectral peak of solid and dashed black lines is due to the chosen charge states for energy calculation. The Au ion flux in the spectrum was calculated by using the absolute calibration of the detector (BAS-TR image plate) response to laser driven Au ions shown in Ref. [16].

efficiently on a plasma populated predominantly by the heavy ions, followed by an efficient acceleration of the Au ion bunch in the transparency regime.

2 Setup

The experiment was performed using the Petawatt arm of the Vulcan laser system at the Rutherford Appleton Laboratory, UK. A schematic of the experimental setup is presented in Fig. 1(a). Linearly polarised beams of central wavelength 1.054 μm were focussed on targets at near-normal incidence (measured as between 1–2°) by an $f/3$ off-axis parabolic mirror, after being reflected off a plasma mirror in order to improve the temporal contrast. Targets consisted of ultra-thin gold foils with thicknesses of 13 ± 5 nm and 30 ± 3 nm (henceforth referred to as 15 nm and 30 nm targets, respectively). The ultra-thin foils were floated-off over washers which are in turn mounted on the target frames. Due to potential target deformations and tilts which can arise during deployment, the incidence angle is typically defined within an uncertainty of a few degrees. The laser energy delivered on target was in the range (175 ± 25) J in (800 ± 100) fs duration, after considering the reflectivity of the plasma mirror (measured experimentally during the campaign). The focal spot had a Gaussian profile, with a full width at half maximum (FWHM) of $\sim$5 μm, and $\sim$35% of the laser energy contained within it, leading to a calculated peak intensity of $(3 \pm 2) \times 10^{20}$ W/cm^2. Three high resolution Thomson parabola spectrometers were deployed along observation lines looking at -5° (TPS1), -1° (TPS2) and 10° (TPS3) with respect to the laser axis, and on the same plane as the interaction. The ion spectra in the TPS were recorded by Fujifilm BAS-TR image plate detectors, whose response to protons, carbon ions and gold ions were absolutely calibrated against CR-39 detectors, as described in Refs. [16, 18–20].

3 Results

Figure 1(e, f, g) shows the Au ion spectra obtained, along each observation line, from the interaction with a 15 nm (black) and a 30 nm (red) thick Au target. Details on the experimental setup can be found in the methods section. The Au traces for similar charge states (typically between 36–55+ for the 15 nm target, and 44–58+ for the 30 nm target) had an unavoidable overlap at energies above a few MeV/n, as can be seen in the traces shown in Fig. 1(b–d). The gold ion spectra in Fig. 1(e–g) represent a range of charge states as labelled. The ion traces for both thicknesses were analysed by integrating the entirety of the ion signal (solid lines), and additionally, for the 15 nm target, a second charge range was analysed by selecting the signal within a range of 45–51+. Ion ener-

gies were calculated assuming an average central charge of 44+ for the 15 nm targets full signal, and 51+ for both the 30 nm targets full signal, and 15 nm targets smaller signal range.

In contrast to the broad spectra obtained from the 30 nm targets, one can clearly observe narrow-band spectral peaks of Au ions from the 15 nm thick targets. The spectral peaks are located at the high energy end of their spectra, peaking on TPS1 at $\sim 8^{+4}_{-2}$ MeV/n. Errors in energy in this instance result from the range of overlapping charge states at high energies, as labelled in the legend in Fig. 1. Using this spectrum, the Au ion bunch across the full charge range (spanning 5–10 MeV/n) is calculated to have a flux of $\sim 8 \times 10^{11}$ particles per steradian [16] — many orders of magnitude higher than the fluxes of GeV Au ions previously reported [8, 11, 15]. The narrow-band spectral peaks are observed predominantly along target-normal (laser-axis) directions (TPS1 and TPS2). In the TPS spectra collected at the widest observation angle (Fig. 1(g), 10°), the prominent gold bunch has faded out both in terms of flux and prominence, with a significant drop in cut-off energy. This indicates that the bunched gold ion beam is produced with a small angular divergence, with a half-cone angle of ∼10–15°.

4 Simulations

The physics underpinning the bunched acceleration of Au ions is explored via 2D PIC simulations employing the fully relativistic code EPOCH [21]. Details on the simulation setup can be found in the Methods section. A linearly polarised pulse with $\lambda = 1.054$ μm, $I_0 = 1.1 \times 10^{20}$ W/cm^2, a Gaussian temporal profile of 700 fs (FWHM), and a Gaussian spot of 5.6 μm (FWHM) was launched along the **x** axis. A target was placed normal to the laser direction, consisting of gold at a density of $58n_c$ (where n_c is the critical density of the laser) at thicknesses of 15 nm and 30 nm, with 10 nm of hydrocarbon contaminants on both the front and rear surfaces. The contaminants contained carbon and hydrogen in the ratio CH_2, with densities of $20n_c$ and $40n_c$, respectively. Due to the many possible heavy ion charge states that can be present in such an interaction, dynamic ionisation was employed, using ionisation energies found on the NIST database [22]. The simulation box was 110 μm in **x**, and 80 μm in **y** with a spatial resolution of 5 nm, and 10 nm, respectively. There was 500 particles per cell and per species, loaded initially into the simulation.

Fig. 2 shows the results of the simulations. The 15 nm target produced a gold bunch, accelerated up to the high energy end of the spectrum, with bunching maintained until after the pulse. Targets thinner than 15 nm resulted in a higher maximum energy of gold ions, however with no apparent spectral peaks at the end of the simulation. Panels (a) and (b) show the time evolution of the cycle averaged longitudinal electric field taken

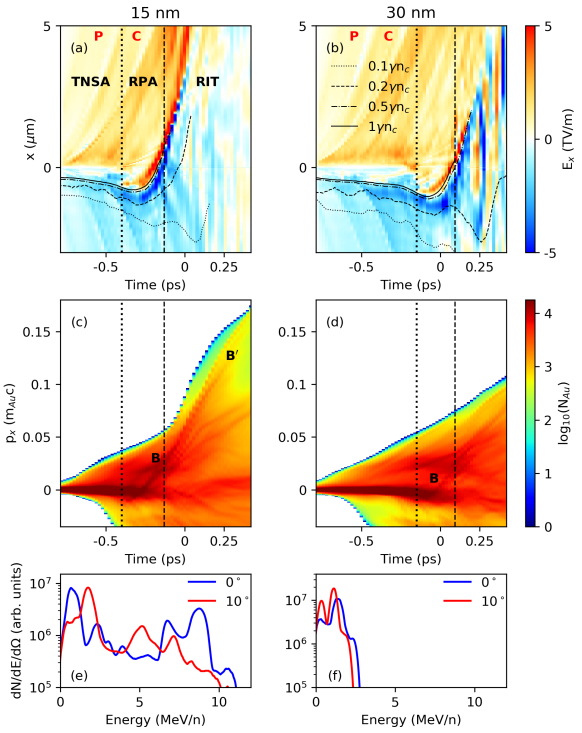

Figure 2: 2D PIC simulations comparing two target thicknesses, showing **(a,b)** the time evolution of the cycle averaged longitudinal electric field along the laser axis for 15 nm and 30 nm thick targets, respectively. The black curves indicate the positions of (relativistically corrected) electron density fronts at 0.1, 0.2, 0.5, and 1 times critical, while the vertical dotted and dashed lines indicate the transitions between each acceleration phase: TNSA, RPA, and RIT. **(c,d)** The time evolution of the Au ion momentum spectrum (integrated over all charge states, to account for ionisation during the pulse) along the laser axis, for each thickness. Time is measured relative to the incidence of the pulse peak at the initial target front surface (x=0 μm). Au^{40-51+} ion energy spectra from the 15 nm **(e)** and 30 nm **(f)** targets are shown, taken at $t = 270$ fs, inside 1 degree half-angle cones directed on-axis (blue — 0°) and off-axis (red — 10°).

along a thin 0.2 μm slice centred on the laser axis. The longitudinal positions of various electron densities are also shown in greyscale on each plot. There are distinct phases of acceleration apparent in the electric field profiles. The initial acceleration during the pulse rising edge is dominated by sheath fields, leading to an ordering of the proton, carbon, and gold ions according to charge-mass ratio, the boundaries between which can be seen in the plot as the sharp jumps in field strength, marked as 'P', and 'C', respectively. At this early stage of the interaction the laser is not intense enough for its radiation pressure to dominate the acceleration. The thermal pressure by the expanding plasma slightly overcomes the radiation pressure, forcing the critical density surface (the

black line on Fig. 2(a) and (b)) backwards. As this thermal expansion causes the electron density of the target plasma to decrease over time, the influence of radiation pressure from the continuously rising pulse intensity begins to take effect. At a certain point (indicated by the dotted lines on each plot) the radiation pressure begins to dominate over the thermal pressure, resulting in the critical surface and bulk plasma ions being accelerated forward (at this point consisting mostly of low q/m ions, such as high charge state gold ions) before the onset of RIT effectively shuts the RPA off. The onset of transparency, corresponding to the time at which maximum $\gamma n_c < 1$, is highlighted by the dashed lines on each plot. The relatively short RPA-dominant phase is what causes the heavy ion bunching, as can be seen in the time evolution of the gold ion spectra (marked as '**B**' in Fig. 2(c) and (d)), before being post-accelerated by transparency-enhanced accelerating fields.

Fig. 2(e) and (f) show Au^{40-51+} ion spectra taken at 270 fs after the pulse peak interaction, for each target thickness. Significant Au ion bunching can be seen for the 15 nm target in the on-axis direction, while for the off-axis direction, the bunching of Au ions has been less effective, showing significantly less prominent spectral peaks with lower fluxes and at lower energies, consistent with the experimental observations. On the other hand, the 30 nm target displays ions with a spectrum devoid of significant peaked features, at a considerably lower energy, and with a more isotropic emission, as was seen in the experiment.

5 Conclusion

In conclusion, we have reported on the first experimental observation of narrowband beams of super heavy ions, at energies approaching 2 GeV and with particle fluxes many orders of magnitude higher than what has previously been reported for laser produced heavy ions. While PIC simulations suggest a complex multi-mechanism, multi-species hybrid scenario behind the formation of narrow-band heavy ions, significant increases in energy can be achieved at upcoming multi-PW laser facilities. These beams could be extremely useful in many applications, most notably in nuclear physics and laboratory astrophysics research.

References

[1] Andrea Macchi, Marco Borghesi, and Matteo Passoni. Ion acceleration by superintense laser-plasma interaction. *Rev. Mod. Phys.*, 85(2):751–793, 2013. ISSN 00346861. doi: 10.1103/RevModPhys.85.751.

[2] Hiroyuki Daido, Mamiko Nishiuchi, and Alexander S Pirozhkov. Review of laser-driven ion sources and their applications. *Rep. Prog. Phys.*, 75(5): 056401, 2012. ISSN 1361-6633. doi: 10.1088/0034-4885/75/5/056401.

[3] Ute Linz and Jose Alonso. Laser-driven ion accelerators for tumor therapy revisited. *Phys. Rev. Accel. Beams*, 19:124802, Dec 2016. doi: 10.1103/PhysRevAccelBeams.19.124802.

[4] R. A. Snavely, B. Zhang, K. Akli, Z. Chen, R. R. Freeman, P. Gu, S. P. Hatchett, D. Hey, J. Hill, M. H. Key, Y. Izawa, J. King, Y. Kitagawa, R. Kodama, A. B. Langdon, B. F. Lasinski, A. Lei, A. J. MacKinnon, P. Patel, R. Stephens, M. Tampo, K. A. Tanaka, R. Town, Y. Toyama, T. Tsutsumi, S. C. Wilks, T. Yabuuchi, and J. Zheng. Laser generated proton beam focusing and high temperature isochoric heating of solid matter. *Phys. Plasmas*, 14 (9), 2007. ISSN 1070664X. doi: 10.1063/1.2774001.

[5] N. V. Zamfir. Nuclear Physics with 10 PW laser beams at Extreme Light Infrastructure - Nuclear Physics (ELI-NP). *European Physical Journal: Special Topics*, 223(6):1221–1227, 2014. ISSN 19516401. doi: 10.1140/epjst/e2014-02176-0.

[6] D. Habs, P. G. Thirolf, M. Gross, K. Allinger, J. Bin, A. Henig, D. Kiefer, W. Ma, and J. Schreiber. Introducing the fission-fusion reaction process: Using a laser-accelerated Th beam to produce neutron-rich nuclei towards the N=126 waiting point of the r-process. *Applied Physics B: Lasers and Optics*, 103(2):471–484, 2011. ISSN 09462171. doi: 10.1007/s00340-010-4261-x.

[7] Sasi Palaniyappan, Chengkun Huang, Donald C. Gautier, Christopher E. Hamilton, Miguel A. Santiago, Christian Kreuzer, Adam B. Sefkow, Rahul C. Shah, and Juan C. Fernández. Efficient quasi-monoenergetic ion beams from laser-driven relativistic plasmas. *Nat. Commun.*, 6, 2015. ISSN 20411723. doi: 10.1038/ncomms10170.

[8] Pengjie Wang, Zheng Gong, Seong Geun Lee, Yinren Shou, Yixing Geng, Cheonha Jeon, I Jong Kim, Hwang Woon Lee, Jin Woo Yoon, Jae Hee Sung, Seong Ku Lee, Defeng Kong, Jianbo Liu, Zhusong Mei, Zhengxuan Cao, Zhuo Pan, Il Woo Choi, Xueqing Yan, Chang Hee Nam, and Wenjun Ma. Super-Heavy Ions Acceleration Driven by Ultrashort Laser Pulses at Ultrahigh Intensity. *Physical Review X*, 11(2):21049, 2021. ISSN 2160-3308. doi: 10.1103/physrevx.11.021049. URL `https://doi.org/10.1103/PhysRevX.11.021049`.

[9] M. Nishiuchi, H. Sakaki, T. Zh Esirkepov, K. Nishio, T. A. Pikuz, A. Ya Faenov, I. Yu Skobelev, R. Orlandi, H. Sako, A. S. Pirozhkov, K. Matsukawa, A. Sagisaka, K. Ogura, M. Kanasaki, H. Kiriyama, Y. Fukuda, H. Koura, M. Kando, T. Yamauchi,

Y. Watanabe, S. V. Bulanov, K. Kondo, K. Imai, and S. Nagamiya. Acceleration of highly charged GeV Fe ions from a low-Z substrate by intense femtosecond laser. *Physics of Plasmas*, 22(3):1–9, 2015. ISSN 10897674. doi: 10.1063/1.4913434.

[10] M. Nishiuchi, N. P. Dover, M. Hata, H. Sakaki, Ko. Kondo, H. F. Lowe, T. Miyahara, H. Kiriyama, J. K. Koga, N. Iwata, M. A. Alkhimova, A. S. Pirozhkov, A. Ya. Faenov, T. A. Pikuz, A. Sagisaka, Y. Watanabe, M. Kando, K. Kondo, E. J. Ditter, O. C. Ettlinger, G. S. Hicks, Z. Najmudin, T. Ziegler, K. Zeil, U. Schramm, and Y. Sentoku. Dynamics of laser-driven heavy-ion acceleration clarified by ion charge states. *Physical Review Research*, 2(3):33081, 2020. ISSN 0031-899X. doi: 10.1103/physrevresearch.2.033081. URL `https://doi.org/10.1103/PhysRevResearch.2.033081`.

[11] F H Lindner, E McCary, X Jiao, T M Ostermayr, R Roycroft, G Tiwari, B M Hegelich, J Schreiber, and P G Thirolf. En-route to the fission–fusion reaction mechanism: a status update on laser-driven heavy ion acceleration. *Plasma Physics and Controlled Fusion*, 61(5):055002, mar 2019. doi: 10.1088/1361-6587/ab068d. URL `https://doi.org/10.1088/1361-6587/ab068d`.

[12] J. Braenzel, A. A. Andreev, K. Platonov, M. Klingsporn, L. Ehrentraut, W. Sandner, and M. Schnürer. Coulomb-Driven Energy Boost of Heavy Ions for Laser-Plasma Acceleration. *Phys. Rev. Lett.*, 114(12):124801, Mar 2015. ISSN 1079-7114. doi: 10.1103/PhysRevLett.114.124801.

[13] M. Tayyab, S. Bagchi, J. A. Chakera, D. K. Avasthi, R. Ramis, A. Upadhyay, B. Ramakrishna, T. Mandal, and P. A. Naik. Mono-energetic heavy ion acceleration from laser plasma based composite nanoaccelerator. *Phys. Plasma*, 25(12):123102, Dec 2018. ISSN 1070-664X. doi: 10.1063/1.5053640.

[14] G M Petrov, C Mcguffey, A G R Thomas, K Krushelnick, and F N Beg. Generation of heavy ion beams using femtosecond laser pulses in the target normal sheath acceleration and radiation pressure acceleration regimes. *Physics of Plasmas*, 23 (063108), 2016. doi: 10.1063/1.4953546. URL `http://dx.doi.org/10.1063/1.4953546`.

[15] F. H. Lindner, E. G. Fitzpatrick, D. Haffa, L. Ponnath, A.-K. Schmidt, M. Speicher, B. Zielbauer, J. Schreiber, and P. G. Thirolf. Charge-state resolved laser acceleration of gold ions to beyond 7 MeV/u. *Sci. Rep.*, 12(4784):1–11, Mar 2022. ISSN 2045-2322. doi: 10.1038/s41598-022-08556-8.

[16] D. Doria, P. Martin, H. Ahmed, A. Alejo, M. Cerchez, S. Ferguson, J. Fernandez-Tobias, J. S. Green, D. Gwynne, F. Hanton, J. Jarrett, D. A. Maclellan, A. McIlvenny, P. McKenna, J. A. Ruiz, M. Swantusch, O. Willi, S. Zhai, M. Borghesi, and S. Kar. Calibration of BAS-TR image plate response to GeV gold ions. 2022. Manuscript accepted for publication. Available at: `https://arxiv.org/abs/2202.10385`.

[17] S. Kar, K. F. Kakolee, B. Qiao, A. Macchi, M. Cerchez, D. Doria, M. Geissler, P. McKenna, D. Neely, J. Osterholz, R. Prasad, K. Quinn, B. Ramakrishna, G. Sarri, O. Willi, X. Y. Yuan, M. Zepf, and M. Borghesi. Ion acceleration in multispecies targets driven by intense laser radiation pressure. *Phys. Rev. Lett.*, 109(18):1–5, nov 2012. ISSN 00319007. doi: 10.1103/PhysRevLett.109.185006.

[18] A. Mančić, J. Fuchs, P. Antici, S. A. Gaillard, and P. Audebert. Absolute calibration of photostimulable image plate detectors used as (0.5-20 MeV) high-energy proton detectors. *Rev. Sci. Instrum.*, 79(7): 0–6, 2008. ISSN 00346748. doi: 10.1063/1.2949388.

[19] D. Doria, S. Kar, H. Ahmed, A. Alejo, J. Fernandez, M. Cerchez, R. J. Gray, F. Hanton, D. A. MacLellan, P. McKenna, Z. Najmudin, D. Neely, L. Romagnani, J. A. Ruiz, G. Sarri, C. Scullion, M. Streeter, M. Swantusch, O. Willi, M. Zepf, and M. Borghesi. Calibration of BAS-TR image plate response to high energy (3-300 MeV) carbon ions. *Rev. Sci. Instrum.*, 86(12), 2015. ISSN 10897623. doi: 10.1063/1.4935582.

[20] A. Alejo, S. Kar, H. Ahmed, A. G. Krygier, D. Doria, R. Clarke, J. Fernandez, R. R. Freeman, J. Fuchs, A. Green, J. S. Green, D. Jung, A. Kleinschmidt, C. L S Lewis, J. T. Morrison, Z. Najmudin, H. Nakamura, G. Nersisyan, P. Norreys, M. Notley, M. Oliver, M. Roth, J. A. Ruiz, L. Vassura, M. Zepf, and M. Borghesi. Characterisation of deuterium spectra from laser driven multi-species sources by employing differentially filtered image plate detectors in Thomson spectrometers. *Rev. Sci. Instrum.*, 85(9):0–7, 2014. ISSN 10897623. doi: 10.1063/1.4893780.

[21] T. D. Arber, K. Bennett, C. S. Brady, A. Lawrence-Douglas, M. G. Ramsay, N. J. Sircombe, P. Gillies, R. G. Evans, H. Schmitz, A. R. Bell, and C. P. Ridgers. Contemporary particle-in-cell approach to laser-plasma modelling. *Plasma Phys. Control. Fusion*, 57(11), 2015. ISSN 13616587. doi: 10.1088/0741-3335/57/11/113001.

[22] A. Kramida, Yu. Ralchenko, J. Reader, and NIST ASD Team. NIST Atomic Spectra Database (ver. 5.6.1), [Online]. Available: https://physics.nist.gov/asd. National Institute of Standards and Technology, Gaithersburg, MD., 2018.